

# Enhanced Electrocatalytic Activity by RGO/MWCNTs/NiO Counter Electrode for Dye-sensitized Solar Cells

Majid Raissan Al-bahrani · Waqar Ahmad · Hadja Fatima Mehnane · Ying Chen · Ze Cheng · Yihua Gao

Received: 6 February 2015 / Accepted: 7 April 2015 / Published online: 17 May 2015  
© The Author(s) 2015. This article is published with open access at Springerlink.com

**Abstract** We applied the reduced graphene oxide/multi-walled carbon nanotubes/nickel oxide (RGO/MWCNTs/NiO) nanocomposite as the counter electrode (CE) in dye-sensitized solar cells (DSSCs) on fluorine-doped tin oxide substrates by blade doctor method. Power conversion efficiency (PCE) of 8.13 % was achieved for this DSSCs device, which is higher than that of DSSCs devices using NiO, RGO, and RGO/NiO-CE (PCE = 2.71 %, PCE = 6.77 % and PCE = 7.63 %). Also, the fill factor of the DSSCs devices using the RGO/MWCNTs/NiO-CE was better than that of other CEs. The electron transfer measurement of cyclic voltammetry and electrochemical impedance spectroscopy showed that RGO/MWCNTs/NiO film could provide fast electron transfer between the CE and the electrolyte, and high electrocatalytic activity for the reduction of triiodide in a CE based on RGO/MWCNTs/NiO in a DSSC.

**Keywords** Graphene oxide · Carbon nanotubes · Nickel oxide · Counter electrode · Dye-sensitized solar cells

## 1 Introduction

In recent, the demand for alternative clean and sustainable energy technologies increases worldwide because of the pollution caused by fossil fuels and their advanced exhaustion. Dye-sensitized solar cells (DSSCs) which can convert the sun energy into electricity are believed to be a promising

energy conversion technology. It becomes essential and very important to improve the DSSCs performance such as low production cost, low environmental impact during fabrication, and high energy conversion efficiency [1]. In the case of the original Grätzel design, the DSSC has three primary parts: photoanode, liquid electrolytes, and platinum (Pt) deposited on another transparent conducting oxide (TCO) substrate [1, 2]. The photoanode which determines the device efficiency is usually fabricated using TiO<sub>2</sub> due to its large ratio of surface area to volume for dye materials [3–6], and the issues related to the counter electrode (CE) must also be addressed. As known, the CE in DSSCs can quickly transport electrons from the electrode substrate to the electrolyte and effectively catalyze the iodide–triiodide ( $I^-/I_3^-$ ) redox reaction in the electrolyte. However, for long-term stability and cost-effective construction of the DSSCs, Pt-CE suffers from its high price, rarity, and susceptibility to corrosion by iodide electrolyte. Using alternative materials of Pt in CE is expected to reduce fabrication cost of DSSCs. Nanocarbon, carbon black, hard carbon spherules, polymer, polymer/Pt, and polymer/carbon have been introduced as catalysts for DSSCs [7–17]. Carbonaceous materials are highly important materials in either their pristine or their

---

M. R. Al-bahrani · W. Ahmad · Y. Chen · Y. Gao (✉)  
Center for Nanoscale Characterization & Devices, Wuhan  
National Laboratory for Optoelectronics, School of Physics,  
Huazhong University of Science and Technology,  
Wuhan 430074, People's Republic of China  
e-mail: gaoyihua@hust.edu.cn

M. R. Al-bahrani  
Faculty of Science, Thi-Qar University, Nasiriyah, Iraq

H. F. Mehnane  
School of Physics and Technology and Key Laboratory of  
Artificial Micro- and Nano-structure of Ministry of Education,  
Wuhan University, Wuhan 430072, People's Republic of China

Z. Cheng  
School of Physics, Huazhong University of Science and  
Technology, Wuhan 430074, People's Republic of China

composite forms due to their low cost and abundance [18–23]. Single-walled carbon nanotubes (SWCNTs), multi-walled carbon nanotubes (MWCNTs), multi-walled carbon nanotubes/graphene (MWCNTs/G), MWCNTs/polymers, and MWCNTs/Pt-CE in DSSCs have been considered as ideal alternative sources to Pt owing to their good properties such as high conductivity, large specific surface area, and chemical stability [24–29]. Recently, Wang et al. prepared a nickel oxide (NiO)-coated fluorine-doped tin oxide (FTO) glass CE in DSSCs, in which NiO was taken as a catalytic role towards  $I^-/I_3^-$  redox couple [30]. The conductive behaviors of metal oxide with CNTs (or graphene) as the CE have been investigated and an increase of the power conversion efficiencies was observed [31, 32]. Yeh et al. demonstrated that reduced graphene oxide (RGO) with good electrocatalytic ability for reducing  $I_3^-$  is a promising catalyst for the CE of DSSCs [33]. However, hybrid materials such as graphene/cobalt sulfide [34] and RGO/Cu<sub>2</sub>S [35] have been reported to show improved catalytic activity and conductivity relative to single-component materials which enhanced efficiency in DSSCs. A RGO/MWCNTs/NiO nanocomposite would be an excellent candidate as counter electrode material for DSSCs.

In this work, we used the RGO/MWCNTs/NiO nanocomposite as a cathode material in DSSCs for catalyzing the  $I^-/I_3^-$  redox reaction and transporting electrons from the FTO to the electrolyte. The combination of high electrocatalytic of NiO and outstanding conductivity of graphene and MWCNTs showed superior performance. Cyclic voltammetry (CV) and electrochemical impedance spectroscopy (EIS) confirmed that the RGO/MWCNTs/NiO-CE has electrocatalytic ability to reduce  $I_3^-$ , and the charge-transfer resistance ( $R_{ct}$ ) was lower. Due to the high catalytic activity and the superior electrical conductivity, the RGO/MWCNTs/NiO-CE also showed excellent photovoltaic performance.

## 2 Experimental

### 2.1 Chemicals and Materials

In this work, the materials and solvents were purchased from Sinopharm Chemical Reagent Co. MWCNTs and graphene oxide (GO) were bought from Beijing Boyu-Gaoke New Material Technology Co. TiO<sub>2</sub> paste and ruthenium 535-bis-TBA (N719) were purchased from Solaronix. The electrolyte was produced by a solution of 0.05 M I<sub>2</sub>, 0.1 M LiI (Adamas-beta), 0.6 M 1-methyl-3-butylimidazolium iodide (TCl), 0.1 m guanidinium thiocyanate (TCl), and 0.5 M 4-tert-butylpyridine (TCl) mixed in 3-methoxypropionitrile solution (Alfa Aesar). Millipore water (18.25 M $\Omega$  cm) was used in the whole process. FTO

glass with a sheet resistance of 8  $\Omega$ /square and a thickness of 2.2 mm, supplied by Nippon Sheet Glass, was used for both electrodes.

### 2.2 Preparation of Counter Electrode

CE for the DSSCs was prepared on coated FTO glass substrate. Firstly, glass substrates coated with FTO were washed with detergent solution and rinsed with deionized (DI) water, and then cleaned in an ultrasonic bath for 15 min in the end rinsed with ethanol and dried in air. Before that, the RGO/MWCNTs/NiO composite was prepared in the following steps as illustrated in Fig. 1. MWCNTs (0.02 g) were refluxed with HNO<sub>3</sub> at 80 °C for 6 h and GO (80 mL) suspension with a concentration of 1 mg mL<sup>-1</sup> under strong stirring. At room temperature, 50 mL aqueous solution containing 0.4362 g nickel (II) nitrate hexahydrate (Ni(NO<sub>3</sub>)<sub>2</sub>·6H<sub>2</sub>O) and 1.5 g urea was slowly dropped into the GO and CNTs suspension with stirring for 30 min. Then, the mixture was refluxed at 100 °C for 12 h in an oil bath. The reaction product was filtered and washed with DI water and ethanol successively several times. Finally, it was dried at 60 °C for 24 h and then heat treated at 250 °C for 2 h in air. To prepare the RGO/MWCNTs/NiO paste, 1 g RGO/MWCNTs/NiO powder was mixed with 0.5 g ethyl cellulose in 8 mL ethanol. Then 0.2 mL acetic acid and 3 g terpeneol were slowly added with continuous mixing for 36 h. To prepare the RGO/MWCNTs/NiO-CE, the RGO/MWCNTs/NiO paste was coated on the FTO glass substrate by the doctor-blade method. Then the formed films were annealed at 400 °C for 30 min using a muffle furnace. For comparison, RGO and RGO/NiO were also prepared under the same synthesis conditions.

### 2.3 DSSC Device Fabrication

For synthesis of the photoanode, TiO<sub>2</sub> layer-by-layer hierarchical nanosheets (TiO<sub>2</sub> LHNs) and their paste were fabricated according to the previously reported method [36, 37]. Briefly, the TiO<sub>2</sub> LHNs powder (0.9 g) was added to the solution containing ethanol/DI water (4:1, volume) and acetylacetone (0.16 mL) for a 3 h stir. After that, TiO<sub>2</sub> paste was applied on pre-treated FTO glass by the doctor-blade method and sintered at 500 °C for 30 min to achieve crystallization in a muffle furnace. The TiO<sub>2</sub> electrode was kept in a dye sensitization (0.5 mM in a mixture of 1:1 acetonitrile/tert-butanol) for at least 12 h at 60 °C in a sealed beaker, then rinsed with ethanol, and dried under nitrogen flow. The TiO<sub>2</sub> photoanode was assembled with the CE manufactured as in Fig. 2a. The electrolyte solution was inserted through holes drilled in the CE, and the holes were sealed with hot-melt film and a cover glass finally.

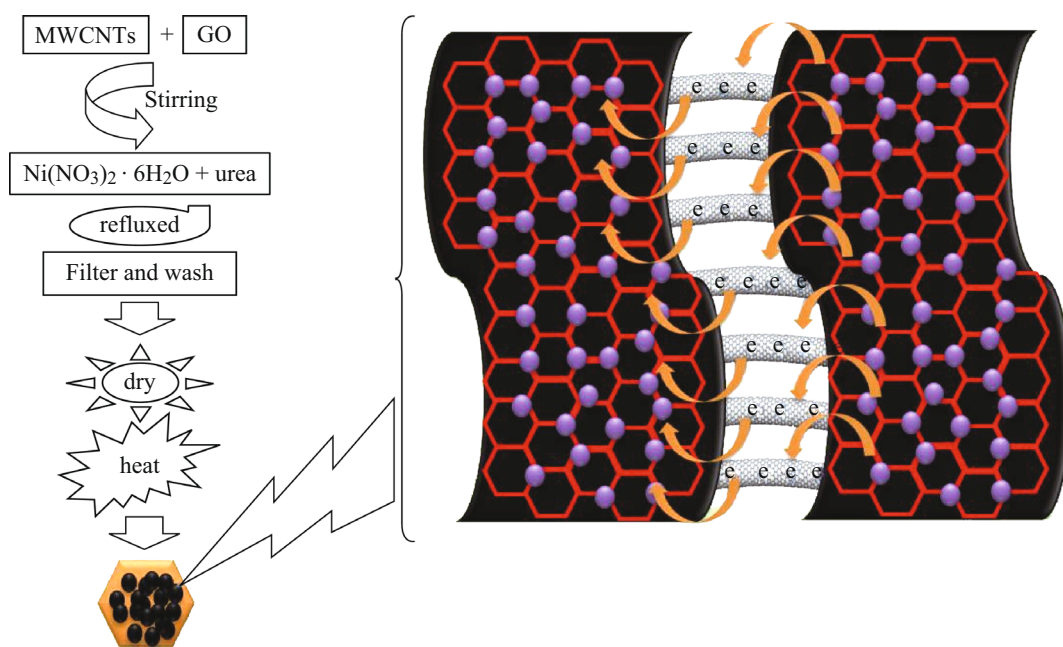


**Fig. 1** Schematic flowchart showing the fabrication process for RGO/MWCNTs/NiO composite

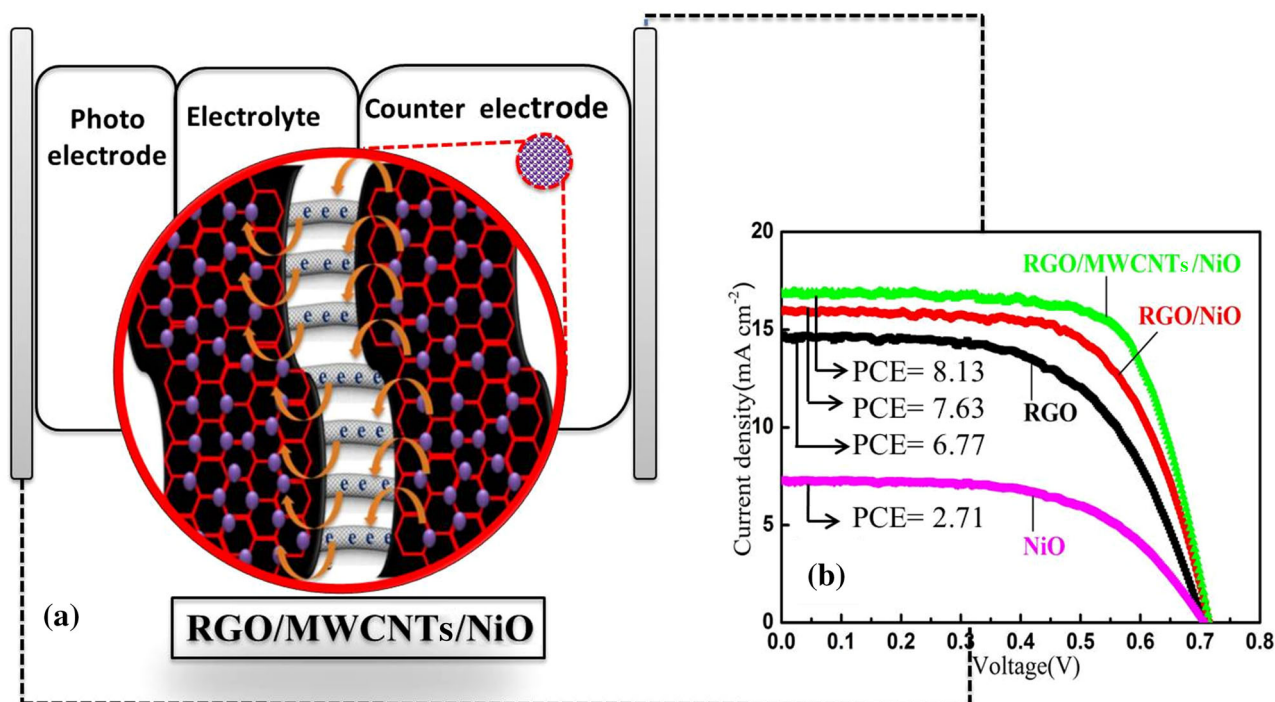


**Fig. 2** a Schematic illustration of a DSSCs device using RGO/MWCNTs/NiO-CE b The current–voltage characteristic curves of DSSC fabricated with different CEs

#### 2.4 Measurements of DSSCs

The morphologies and structures of the samples were characterized using high-resolution field emission scanning electron microscopy (SEM, FEI Nova Nano-SEM 450), transmission electron microscopy (TEM, Tecnai G2 20

U-Twin), and X-ray diffractometer (XRD, PANalytical B.V. X'Pert PRO). The redox properties of dye were examined by cyclic voltammetry at a scan rate of 50 mV s<sup>-1</sup>. The electrolyte solution was an acetonitrile solution containing 10 mM LiI, 5 mM I<sub>2</sub>, and 0.1 M LiClO<sub>4</sub>. Tests were conducted in a three-electrode one-compartment cell,

where CE, Pt, and Ag/AgCl were taken as the working electrode, auxiliary electrode, and reference electrode, respectively. The photovoltaic current density–voltage ( $J$ – $V$ ) characteristics of the prepared DSSCs were measured under illumination conditions ( $100 \text{ mW cm}^{-2}$ , AM 1.5), which was verified using Si photodiode, solar-simulator illumination (Newport, USA) on the active cell area of  $0.15 \text{ cm}^2$ . The light-to-electric power conversion efficiency (PCE) and fill factor (FF) were calculated according to the equations [38]:

$$\text{FF} = \frac{V_{\text{max}} \times J_{\text{max}}}{V_{\text{oc}} \times J_{\text{sc}}} \quad (1)$$

$$\text{PCE} = \frac{V_{\text{max}} \times J_{\text{max}}}{P_{\text{in}}} \times 100 \% = \frac{V_{\text{oc}} \times J_{\text{sc}} \times \text{FF}}{P_{\text{in}}} \times 100 \% \quad (2)$$

where  $V_{\text{max}}$  and  $J_{\text{max}}$  are, respectively, the voltage and the current density under the maximum power output in the  $J$ – $V$  curves,  $J_{\text{sc}}$  is the short-circuit current density ( $\text{mA cm}^{-2}$ ),  $V_{\text{oc}}$  is the open-circuit voltage (V), and  $P_{\text{in}}$  is the incident light power. EIS was examined at the open-circuit potential under the same illumination condition as the measurement of the  $J$ – $V$  curves. The data were obtained by using Z-view software NOVA 1.7 to analyze the results from Auto-lab electrochemical work station (model AUT84315, the Netherlands) [39].

### 3 Results and Discussion

Figure 3 shows SEM and TEM images of RGO/MWCNTs/NiO nanocomposites. NiO nanoparticles were anchored on the surface of RGO sheets, which were separated by MWCNTs with less aggregation. From TEM images, NiO nanoparticles with uniform size were distributed on the surface of the RGO and connected by MWCNTs to form continuous network (Fig. 3c, d). More active sites were available in this structure, and electron transport properties as well as the cell performance are expected to be improved.

Thermo gravimetric analysis (TGA) measurements were carried out to determine the mass ratio of RGO/MWCNTs/NiO composites (Fig. 3f). The first step occurred around  $\sim 200 \text{ }^\circ\text{C}$ , which was due to the removal of the physisorbed water. The large weight loss below  $\sim 400 \text{ }^\circ\text{C}$  was attributed to the removal of RGO from the composites. Between 400 and  $710 \text{ }^\circ\text{C}$ , the graphitic carbon burnt off accounting for the second burn stage. Above  $710 \text{ }^\circ\text{C}$ , the TGA trace was stable with no further weight loss and only NiO remained.

XRD results of samples are shown in Fig. 4. For MWCNTs, it shows a characteristic diffraction peak at  $2\theta$  of  $26^\circ$  (0 0 2), whereas RGO/MWCNTs/NiO nanocomposite

shows new diffraction peaks at  $37.2^\circ$  (1 1 1),  $42.8^\circ$  (2 0 0), and  $62.4^\circ$  (2 2 0) which ascribe to the crystal structure of NiO nanoparticles. However, no characteristic diffraction peak of GO observed in the RGO/MWCNTs/NiO nanocomposite indicated the successful reduction of GO to RGO.

To study the electrochemical behavior of composites, EIS was conducted under illumination of AM 1.5 G ( $100 \text{ mW cm}^{-2}$ ) and a potential amplitude of 10 mV with frequencies of 10 mHz–100 kHz to understand the effect of the electrocatalytic activities of different CE on the  $\text{I}_3^-$  reduction. The impedance spectra were illustrated as Nyquist plots and the equivalent circuit (Fig. 5). These works focus on the semicircle in the highest frequency region describing the electron transport at the CE/electrolyte interface. The charge-transfer resistance ( $R_{\text{ct}}$ ) occurs at the contact interface between the electrode and the electrolyte [40].  $R_s$  is the series resistance including the TCO's sheet resistance and the cell's contact resistances as itemized in Table 1. It can be seen that RGO/MWCNTs/NiO-CE has the smallest diameter of semicircle which was related to the less  $R_{\text{ct}}$  ( $0.9 \text{ } \Omega$ ), whereas RGO and NiO-CE have the largest  $R_{\text{ct}}$  (2.3 and  $4.7 \text{ } \Omega$ ). When NiO nanoparticles were adopted with RGO, the  $R_{\text{ct}}$  decreased to  $1.3 \text{ } \Omega$  and the DSSC device with the RGO/MWCNTs/NiO-CE exhibits the smallest  $R_{\text{ct}}$ , indicating the optimal compositions of RGO/NiO and MWCNTs. Since  $R_{\text{ct}}$  of the CE affects the FF and PCE of DSSCs in a negative way [41–43], indicating the improved electrocatalytic activity for redox electrolyte and high electron transfer kinetics, it will lead to a greater diffusion of the iodide/triiodide ( $\text{I}^-/\text{I}_3^-$ ) from the bulk solution to the electrode surface.

In order to understand further the improved DSSC devices with RGO/MWCNTs/NiO-CE, we measured CV curves of the  $\text{I}^-/\text{I}_3^-$  redox couple on the RGO/MWCNTs/NiO, RGO/NiO and RGO CE, respectively. From the results shown in Fig. 6, two sets of peaks were observed, which is due to the redox reaction of the  $\text{I}^-/\text{I}_3^-$  redox shuttle and another redox reaction of the  $\text{I}_3^-/\text{I}_2^-$  redox couple [44]. It is well known that two key parameters for estimating the catalytic activities of the CE are the peak-to-peak separation ( $E_{\text{pp}}$ ) and peak current density ( $I_{\text{p}}$ ) [45]. Therefore, the magnitude of  $I_{\text{p}}$  is proportional to the ability of the CE to reduce the  $\text{I}_3^-$  species, while the magnitude of  $E_{\text{pp}}$  is inversely proportional to the ability of the CE to reduce the  $\text{I}_3^-$  species. The CE in the DSSC is responsible for catalyzing the regeneration of  $\text{I}^-$  from  $\text{I}_3^-$  ( $\text{I}_3^- + 2\text{e}^- \rightarrow 3\text{I}^-$ ) [46]. The RGO/MWCNTs/NiO electrode shows larger  $I_{\text{p}}$  (2.88 mA) from the redox reaction of the  $\text{I}^-/\text{I}_3^-$  redox shuttle than the other two electrodes with the RGO and RGO/NiO electrodes showing  $I_{\text{p}}$  of 1.18 and 2.4 mA, respectively (Table 2). In addition,  $E_{\text{pp}}$  of RGO/MWCNTs/NiO-CE was lower than those of the RGO and RGO/NiO-CE. The RGO/MWCNTs/NiO-CE offers a high

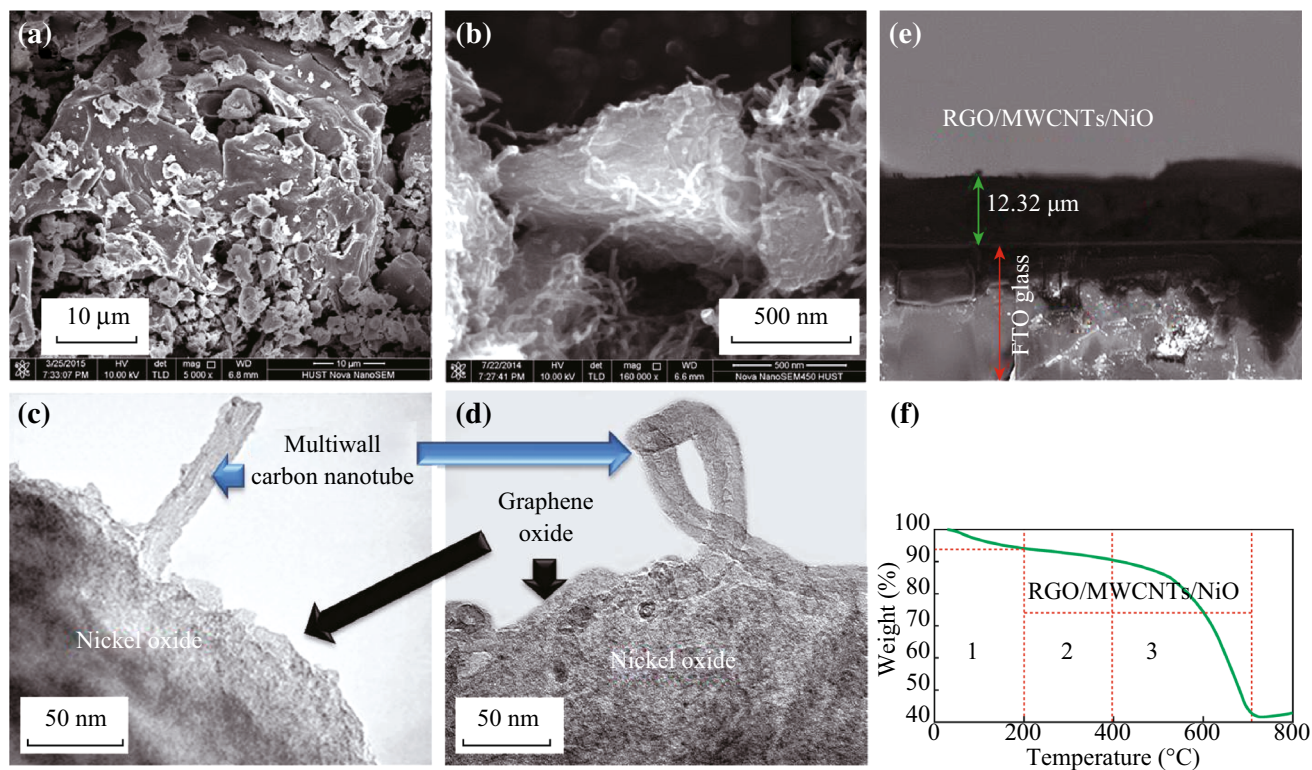


**Fig. 3** a–d SEM and TEM images of RGO/MWCNTs/NiO composite. e SEM image of RGO/MWCNTs/NiO film on FTO glass substrate (cross section), showing the thickness of the film. f The TGA analysis of the RGO/MWCNTs/NiO

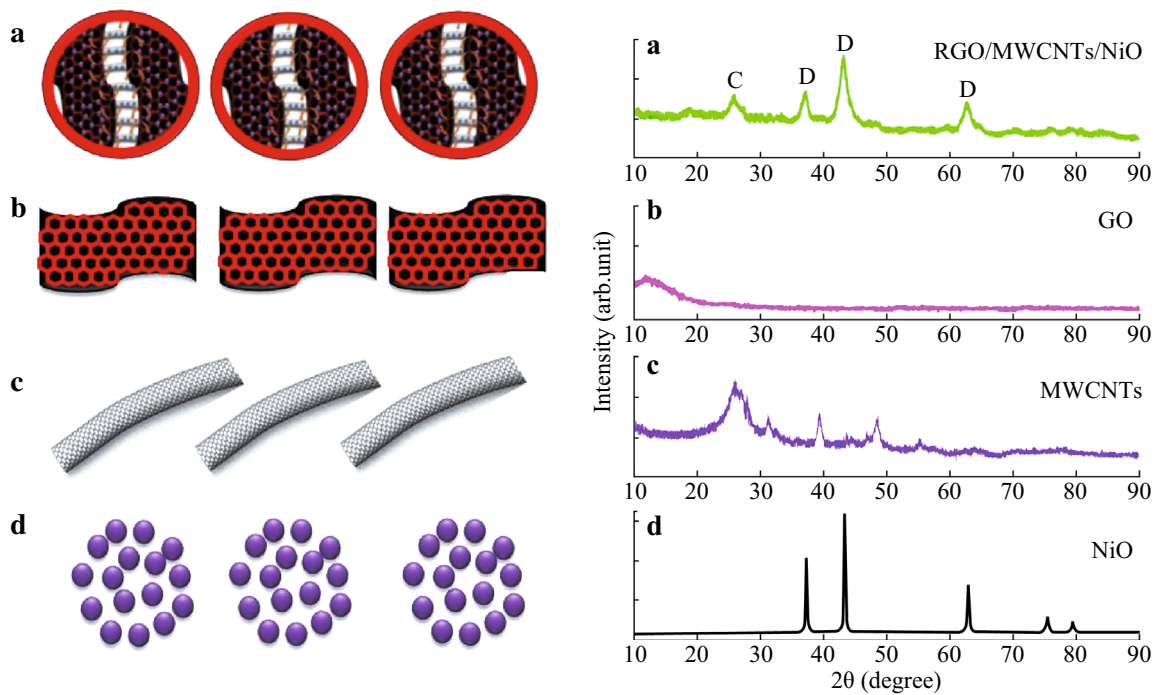


**Fig. 4** XRD patterns of GO-, NiO-, MWCNTs-, and RGO/MWCNTs/NiO-CE

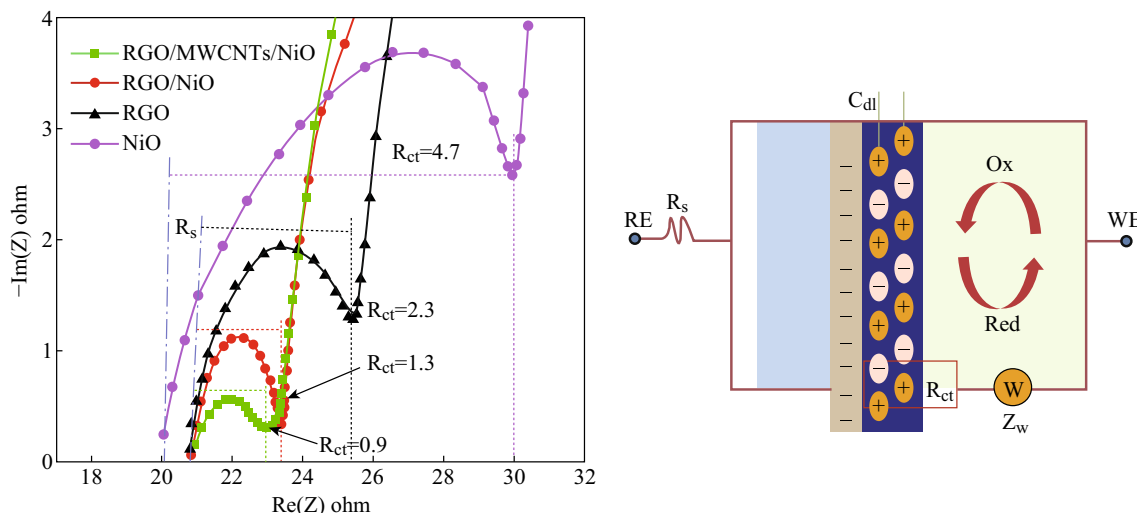


**Fig. 5** EIS analysis of RGO-, RGO/NiO-, and RGO/MWCNTs/NiO-CE and equivalent circuit models. ( $R_s$ ,  $R_{ct}$ ,  $C_{dl}$ , and  $Z_w$  are serial resistance, charge-transfer resistance of electrode, double layer capacitance, and diffusion impedance, respectively)

**Table 1** Photovoltaic performance of RGO-, RGO/NiO-, and RGO/MWCNTs/NiO-CE based DSSCs prepared by doctor-blade method

Counter electrode	$J_{sc}$ ( $\text{mA cm}^{-2}$ )	$V_{oc}$ (V)	FF	PCE (%)	$R_s$ ( $\Omega$ )	$R_{ct}$ ( $\Omega$ )
NiO	7.31	0.70	0.53	2.71	20.02	4.7
RGO	14.36	0.70	0.67	6.77	20.67	2.3
RGO/NiO	15.86	0.71	0.67	7.63	20.71	1.3
RGO/MWCNTs/NiO	16.80	0.71	0.68	8.13	20.62	0.9

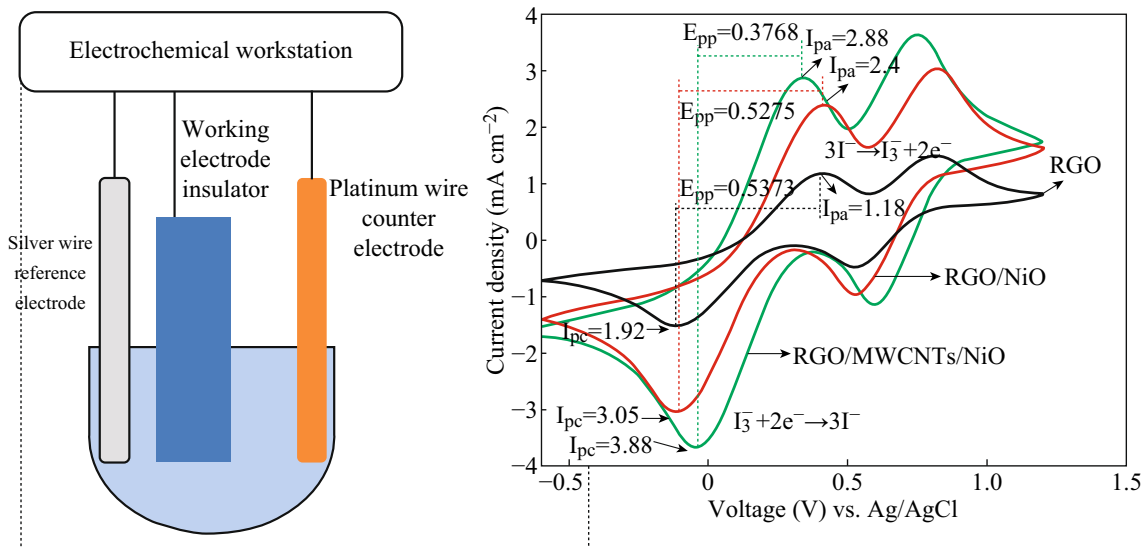


**Fig. 6** Cyclic voltammograms for RGO, RGO/NiO, and RGO/MWCNTs/NiO electrodes. The electrolyte was acetonitrile solution containing 10 mM LiI, 5 mM  $I_2$ , and 0.1 M  $LiClO_4$ . Pt electrode was used as auxiliary electrode and Ag/AgCl works as reference electrode. The scan rate is  $50 \text{ mV s}^{-1}$

enough active area for faster and stronger redox reactions and a higher electrocatalytic effect for the reduction of  $I_3^-$  at the RGO/MWCNTs/NiO electrode.

The  $J-V$  curves of photovoltaic performance for DSSCs devices with NiO, RGO, RGO/NiO, and RGO/MWCNTs/NiO different CEs are shown in Fig. 2b. The devices'

**Table 2**  $E_{pp}$ ,  $I_{pa}$ , and  $I_{pc}$  of RGO, RGO/NiO and RGO/MWCNTs/NiO electrodes

Counter electrode	$E_{pp}$	$I_{pa}$ (mA cm <sup>-2</sup> )	$I_{pc}$ (mA cm <sup>-2</sup> )
RGO	0.53	1.18	1.92
RGO/NiO	0.52	2.4	3.05
RGO/MWCNTs/NiO	0.37	2.88	3.88

**Table 3** Photoelectric performances of the DSSCs using various thickness of RGO/MWCNTs/NiO film as CE

Thickness ( $\mu\text{m}$ )	$J_{sc}$ (mA cm <sup>-2</sup> )	$V_{oc}$ (V)	FF	PCE (%)
12.32	16.80	0.71	0.68	8.13
9.16	16.69	0.69	0.64	7.37
4.54	16.18	0.67	0.63	6.82
3.60	16.05	0.70	0.58	6.51

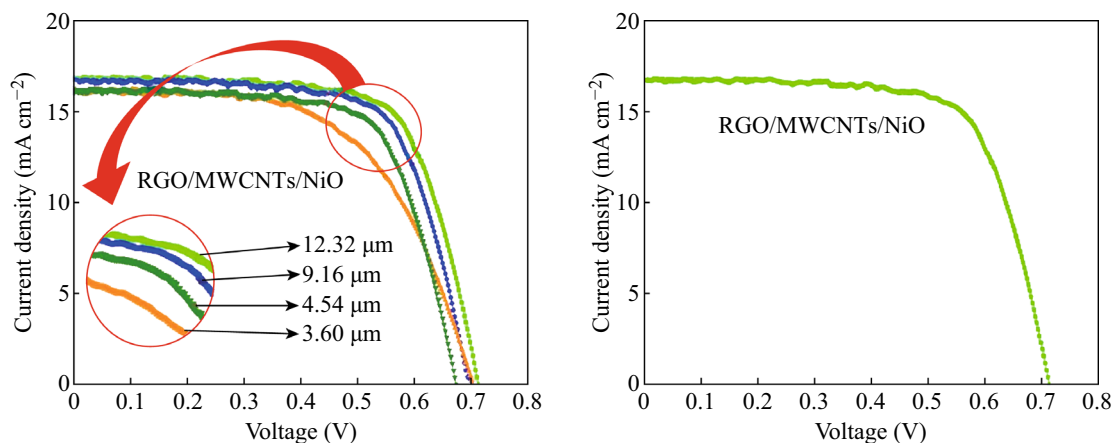
performance parameters including  $J_{sc}$ ,  $V_{oc}$ , FF, and PCE are summarized in Table 1. The PCE and FF were calculated according to the Eqs. (1) and (2). The DSSC devices with RGO/MWCNTs/NiO-CE reach the highest power conversion efficiency. The PCE significantly enhanced from 6.77 % for RGO CE cell to 8.13 % for RGO/MWCNTs/NiO-CE one. This may be due to the increase of electrocatalytic activity toward  $\text{I}^-/\text{I}_3^-$  redox species and decrease of  $R_{ct}$ . From CV curves in Fig. 6 and values of  $J_{sc}$  and PCE in Table 1, the DSSC devices with RGO/MWCNTs/NiO-CE exhibit the best photovoltaic performances, as well as better FF compared with other CEs. The enhanced  $J_{sc}$  maybe results from the enhanced diffusivity of  $\text{I}^-/\text{I}_3^-$  redox species within CE [47]. However, the improved performance should attribute to the incorporation of MWCNTs into RGO/NiO which provides larger space allowing easy diffusion between the redox species.

RGO/MWCNTs/NiO films with different thicknesses of 3.6–12.7  $\mu\text{m}$  were prepared to investigate the film thickness effect on performances of DSSCs (Table 3). As shown in Fig. 7,  $V_{oc}$  and FF increase with the film thickness, whereas  $J_{sc}$  is almost unchangeable. The highest photovoltaic efficiency of 8.13 % was observed in 12.7- $\mu\text{m}$  DSSC (SEM image of the cross section shown in Fig. 3e). The RCT between electrolyte and RGO/MWCNTs/NiO increases with decreasing the film thickness, leading to the decrease of the FF and the PCE of DSSCs [48]. This is due to the insufficient catalytic activity for the reduction of triiodide of the thinner RGO/MWCNTs/NiO layers.

In addition, it should be mentioned that decrease of NiO particle size will enhance the conductivity of RGO/MWCNTs/NiO composites because of the synergistic effect between RGO and MWCNTs. CNTs not only prevent aggregation of RGO/NiO but also improve the electron transport properties of RGO/MWCNTs/NiO composite owing to their special conductivity. Moreover, the restricting effect of RGO makes NiO nanoparticles provide more active sites. It is because of the unique structure and properties, RGO/MWCNTs/NiO composite has enhanced electrochemical performance compared with that of RGO/NiO and MWCNTs/NiO ones.

#### 4 Conclusion

In this paper, we fabricated RGO/MWCNTs/NiO composite and applied it in DSSC as a CE by blade doctor method. High PCE of 8.13 % was achieved in such DSSC, which is much higher than that of NiO (2.71 %), RGO (6.77 %) and RGO/NiO (7.63 %). Also, it was found that the RGO/MWCNTs/NiO-CE has less charge-transfer resistance at the electrolyte/CE interface and higher catalytic activity for reduction of  $\text{I}_3^-$  to  $\text{I}^-$ . The improved

**Fig. 7** The current–voltage curves of DSSCs using different thickness of RGO/MWCNTs/NiO film as counter electrodes

performances maybe attribute to the enhanced electrode conductivity, the increased effective interfacial area between RGO/MWCNTs/NiO and electrolyte, as well as the contact area between RGO/NiO and other materials by MWCNTs.

**Acknowledgments** This work was supported by the National Basic Research Program (2011CB933300) of China, and the National Natural Science Foundation of China (11374110, 11204093, 51371085, and 11304106).

**Open Access** This article is distributed under the terms of the Creative Commons Attribution 4.0 International License (<http://creativecommons.org/licenses/by/4.0/>), which permits unrestricted use, distribution, and reproduction in any medium, provided you give appropriate credit to the original author(s) and the source, provide a link to the Creative Commons license, and indicate if changes were made.

## References

1. B. O'Regan, M. Grätzel, Low-cost, high efficiency solar cell based on dye-sensitized colloidal TiO<sub>2</sub> films. *Nature* **353**, 737–740 (1991). doi:10.1038/353737a0
2. M. Grätzel, Photoelectrochemical cells. *Nature* **414**, 338–344 (2001). doi:10.1038/35104607
3. A. Yella, H.W. Lee, H.N. Tsao, C. Yi, A.K. Chandiran, M.K. Nazeeruddin, E.W.G. Diau, C.Y. Yeh, S.M. Zakeeruddin, M. Grätzel, Porphyrin sensitized solar cells with cobalt (II/III)-based redox electrolyte exceed 12 % efficiency. *Science* **334**(6056), 629–634 (2011). doi:10.1126/science.1209688
4. S. Ito, P. Chen, P. Comte, M.K. Nazeeruddin, P. Liska, P. Péchy, M. Grätzel, Fabrication of screen printing pastes from TiO<sub>2</sub> powders for dye-sensitized solar cells. *Prog. Photovolt. Res. Appl.* **15**(7), 603–612 (2007). doi:10.1002/ppp.768
5. Y. Chiba, A. Islam, Y. Watanabe, R. Komiya, N. Koide, L. Han, Dye-sensitized solar cells with conversion efficiency of 11.1 %. *Jpn. J. Appl. Phys.* **45**(24–28), L638–L640 (2006). doi:10.1143/JJAP.45.L638
6. L. Han, A. Islam, A. Han Chen, C. Malapak, B. Chiranjeevi, S. Zhang, X. Yang, M. Yanagida, High-efficiency dye-sensitized solar cell with a novel co-adsorbent. *Energy Environ. Sci.* **5**, 6057–6060 (2012). doi:10.1039/c2ee03418b
7. Y. Saito, W. Kubo, T. Kitamura, Y. Wada, S. Yanagida, I-/I<sub>3</sub>-redox reaction behavior on poly (3, 4-ethylenedioxythiophene) counter electrode in dye-sensitized solar cells. *J. Photochem. Photobiol. A-Chem.* **164**(1–3), 153–157 (2004). doi:10.1016/j.jphotochem.2003.11.017
8. B. Fan, X. Mei, K. Sun, J. Ouyang, Conducting polymer/carbon nanotube composite as counter electrode of dye-sensitized solar cells. *Appl. Phys. Lett.* **93**, 143103 (2008). doi:10.1063/1.2996270
9. T.N. Murakami, S. Ito, Q. Wang, M.K. Nazeeruddin, T. Bessho, I. Cesar, P. Liska, R. Humphry-Baker, P. Comte, P. Péchy, M. Grätzel, Highly efficient dye-sensitized solar cells based on carbon black counter electrodes. *J. Electrochem. Soc.* **153**(12), A2255–A2261 (2006). doi:10.1149/1.2358087
10. W. Hong, Y. Xu, G. Lu, C. Li, G. Shi, Transparent graphene/PEDOT-PSS composite films as counter electrodes of dye-sensitized solar cells. *Electrochem. Commun.* **10**(10), 1555–1558 (2008). doi:10.1016/j.elecom.2008.08.007
11. K. Imoto, K. Takahashi, T. Yamaguchi, T. Komura, J. Nakamura, K. Murata, High-performance carbon counter electrode for dye-sensitized solar cells. *Sol. Energy Mater. Sol. Cells* **79**(4), 459–469 (2003). doi:10.1016/S0927-0248(03)00021-7
12. Z. Huang, X. Liu, K. Li, D. Li, Y. Luo, H. Li, W. Song, L.-Q. Chen, Q. Meng, Application of carbon materials as counter electrodes of dye-sensitized solar cells. *Electrochem. Commun.* **9**(4), 596–598 (2007). doi:10.1016/j.elecom.2006.10.028
13. E. Ramasamy, *Nanocarbon counter electrode for dye sensitized solar cells*, vol. 90 (AIP, New York, 2007)
14. P. Joshi, L. Zhang, Q. Chen, D. Galipeau, H. Fong, Q. Qiao, Electrospun carbon nanofibers as low-cost counter electrode for dye-sensitized solar cells. *ACS Appl. Mater. Interfaces* **2**(12), 3572–3577 (2010). doi:10.1021/am100742s
15. X. Mei, S.J. Cho, B. Fan, J. Ouyang, High-performance dye-sensitized solar cells with gel-coated binder-free carbon nanotube films as counter electrode. *Nanotechnology* **21**(39), 395202 (2010). doi:10.1088/0957-4484/21/39/395202
16. C.-T. Hsieh, B.-H. Yang, J.-Y. Lin, One- and two-dimensional carbon nanomaterials as counter electrodes for dye-sensitized solar cells. *Carbon* **49**(9), 3092–3097 (2011). doi:10.1016/j.carbon.2011.03.031
17. G. Veerappan, K. Bojan, S.-W. Rhee, Sub-micrometer-sized graphite as a conducting and catalytic counter electrode for dye-sensitized solar cells. *ACS Appl. Mater. Interfaces* **3**(3), 857–862 (2011). doi:10.1021/am101204f
18. L. Kavan, J.H. Yum, M.K. Nazeeruddin, M. Grätzel, Graphene nanoplatelet cathode for Co(III)/(II) mediated dye-sensitized solar cells. *ACS Nano* **5**(11), 9171–9178 (2011). doi:10.1021/nm203416d
19. F. Gong, Z. Li, H. Wang, Z.S. Wang, Enhanced electrocatalytic performance of graphene via incorporation of SiO<sub>2</sub> nanoparticles for dye-sensitized solar cells. *J. Mater. Chem.* **22**, 17321–17327 (2012). doi:10.1039/c2jm33483f
20. A. Kaniyoor, S. Ramaprabhu, Thermally exfoliated graphene based counter electrode for low cost dye sensitized solar cells. *J. Appl. Phys.* **109**, 124308 (2011). doi:10.1063/1.3600231
21. A. Kay, M. Grätzel, Low cost photovoltaic modules based on dye sensitized nanocrystalline titanium dioxide and carbon powder. *Sol. Energy Mater. Sol. Cells* **44**(1), 99–117 (1996). doi:10.1016/0927-0248(96)00063-3
22. K. Suzuki, M. Yamaguchi, M. Kumagai, S. Yanagida, Application of carbon nanotubes to counter electrodes of dye-sensitized solar cells. *Chem. Lett.* **32**(1), 28–29 (2003). doi:10.1246/cl.2003.28
23. W.J. Lee, E. Ramasamy, D.Y. Lee, J.S. Song, Efficient dye-sensitized solar cells with catalytic multiwall carbon nanotube counter electrodes. *ACS Appl. Mater. Interfaces* **1**(6), 1145–1149 (2009). doi:10.1021/am800249k
24. C.S. Du, N. Pan, Supercapacitors using carbon nanotubes films by electrophoretic deposition. *J. Power Sources* **160**(2), 1487 (2006). doi:10.1016/j.jpowsour.2006.02.092
25. H.Y. Wang, F.M. Wang, Y.Y. Wang, C.C. Wan, B.J. Hwang, R. Santhanam, Electrochemical formation of Pt nanoparticles on multiwalled carbon nanotubes: useful for fabricating electrodes for use in dye-sensitized solar cells. *J. Rick J. Phys. Chem. C* **115**(16), 8439–8445 (2011). doi:10.1021/jp201220t
26. H.J. Shin, S.S. Jeon, S.S. Im, CNT/PEDOT core/shell nanostructures as a counter electrode for dye-sensitized solar cells. *Synth. Met.* **161**(13–14), 1284–1288 (2011). doi:10.1016/j.synthmet.2011.04.024
27. M.R. Al-bahrani, X. Xu, W. Ahmad, X.-L. Ren, J. Su, Z. Cheng, Y. Gao, Highly efficient dye-sensitized solar cell with GNS/MWCNT/PANI as a counter electrode. *Mater. Res. Bull.* **59**, 272–277 (2014). doi:10.1016/j.materresbull.2014.07.029
28. L. Chang, C. Lee, K. Huang, Y. Wang, M. Yeh, J. Lin, K. Ho, Facile fabrication of PtNP/MWCNT nanohybrid films for flexible counter electrode in dye-sensitized solar cells. *J. Mater. Chem.* **22**(7), 3185–3191 (2012). doi:10.1039/c2jm15614h

29. I. Ahmad, J.E. McCarthy, M. Bari, Y.K. Gunko, Carbon nanomaterial based counter electrodes for dye sensitized solar cells. *Sol. Energy* **102**, 152–161 (2014). doi:[10.1016/j.solener.2014.01.012](https://doi.org/10.1016/j.solener.2014.01.012)
30. H. Wang, W. Wei, Y.H. Hu, NiO as an Efficient counter electrode catalyst for dye-Sensitized solar cells. *Top Catal.* **57**(6–9), 607–611 (2014). doi:[10.1007/s11244-013-0218-8](https://doi.org/10.1007/s11244-013-0218-8)
31. M.R. Al-bahrani, L. Liu, W. Ahmad, J. Tao, F. Tu, Z. Cheng, Y. Gao, NiO-NF/MWCNT nanocomposite catalyst as a counter electrode for high performance dye-sensitized solar cells. *Appl. Surf. Sci.* **331**, 333–338 (2015). doi:[10.1016/j.apsusc.2015.01.015](https://doi.org/10.1016/j.apsusc.2015.01.015)
32. J.S. Jang, D.J. Ham, E. Ramasamy, J. Lee, J.S. Lee, Platinum-free tungsten carbides as an efficient counter electrode for dye sensitized solar cells. *Chem. Commun.* **46**, 8600–8602 (2010). doi:[10.1039/c0cc02247k](https://doi.org/10.1039/c0cc02247k)
33. M.-H. Yeh, L.-Y. Lin, L.-Y. Chang, Y.-A. Leu, W.-Y. Cheng, J.-J. Lin, K.-C. Ho, Dye-sensitized solar cells with reduced graphene oxide as the counter electrode prepared by a green photochemical reduction process. *Chem. Phys. Chem.* **15**(6), 1175–1181 (2014). doi:[10.1002/cphc.201301128](https://doi.org/10.1002/cphc.201301128)
34. E. Bi, H. Chen, X. Yang, W. Peng, M. Grätzel, L. Han, A quasi core-shell nitrogen-doped graphene/cobalt sulfide conductive catalyst for highly efficient dye-sensitized solar cells. *Energy Environ. Sci.* **7**, 2637–2641 (2014). doi:[10.1039/C4EE01339E](https://doi.org/10.1039/C4EE01339E)
35. E. Bi, Y. Su, H. Chen, X. Yang, M. Yin, F. Ye, Z. Li, L. Han, A hybrid catalyst composed of reduced graphene oxide/Cu<sub>2</sub>S quantum dots as a transparent counter electrode for dye sensitized solar cells. *RSC Adv.* **5**, 9075–9078 (2015). doi:[10.1039/C4RA14029J](https://doi.org/10.1039/C4RA14029J)
36. J. Zhu, J. Wang, F. Lv, S. Xiao, C. Nuckolls, H. Li, Synthesis and self-assembly of photonic materials from nanocrystalline titania sheets. *J. Am. Chem. Soc.* **135**(12), 4719–4721 (2013). doi:[10.1021/ja401334j](https://doi.org/10.1021/ja401334j)
37. W. Sun, T. Peng, Y. Liu, W. Yu, K. Zhang, H.F. Mehnane, C. Bu, S. Guo, X.-Z. Zhao, Layer-by-Layer self-assembly of TiO<sub>2</sub> hierarchical nanosheets with exposed 001 facets as an effective bifunctional layer for dye-sensitized solar cells. *ACS Appl. Mater. Interfaces* **6**(12), 9144–9149 (2014). doi:[10.1021/am501233q](https://doi.org/10.1021/am501233q)
38. M. Grätzel, Perspectives for dye-sensitized nanocrystalline solar cells. *Prog. Photovolt Res. Appl.* **8**(1), 171–185 (2000). doi:[10.1002/\(SICI\)1099-159X\(200001/02\)8:1<171:AID-PIP300>3.0.CO;2-U](https://doi.org/10.1002/(SICI)1099-159X(200001/02)8:1<171:AID-PIP300>3.0.CO;2-U)
39. J.H. Cheon, D.Y. Jung, S.K. Choi, K.-S. Ahn, D.K. Lee, J.H. Kim, Enhancement of light harvesting in dye-sensitized solar cells by using Förster-type resonance energy transfer. *Met. Mater. Int.* **19**(6), 1365–1368 (2013). doi:[10.1007/s12540-013-0642-0](https://doi.org/10.1007/s12540-013-0642-0)
40. F.F. Santiago, J. Bisquert, E. Palomares, Correlation between photovoltaic performance and impedance spectroscopy of dye-sensitized solar cells based on ionic liquids. *Phys. Chem. C* **111**(17), 6550–6560 (2007). doi:[10.1021/jp066178a](https://doi.org/10.1021/jp066178a)
41. S. Das, P. Sudhagar, V. Verma, D. Song, E. Ito, S.Y. Lee, Y. Kang, W. Choi, Amplifying charge-transfer characteristics of graphene for triiodide reduction in dye-sensitized solar cells. *Adv. Funct. Mater.* **21**(19), 3729–3736 (2011). doi:[10.1002/adfm.201101191](https://doi.org/10.1002/adfm.201101191)
42. D.W. Zhang, X.D. Li, H.B. Li, S. Chen, Z. Sun, X.J. Yin, S.M. Huang, Graphene-based counter electrode for dye-sensitized solar cells. *Carbon* **49**(15), 538–5388 (2011). doi:[10.1016/j.carbon.2011.08.005](https://doi.org/10.1016/j.carbon.2011.08.005)
43. L. Han, N. Koide, Y. Chiba, A. Isalam, R. Komiya, N. Fuke, A. Fukui, R. Ymanaka, Improvement of efficiency of dye sensitized solar cells by reduction of internal resistance. *Appl. Phys. Lett.* **86**, 213501–213503 (2005). doi:[10.1063/1.1925773](https://doi.org/10.1063/1.1925773)
44. A. Ejigu, K.R.J. Lovelock, P. Licence, D.A. Walsh, The effect of linker of electrodes prepared from sol-gel ionic liquid precursor and carbon nanoparticles on dioxygen electroreduction bioelectrocatalysis. *Electrochim. Acta* **56**(28), 10306–10313 (2011). doi:[10.1016/j.electacta.2011.03.139](https://doi.org/10.1016/j.electacta.2011.03.139)
45. F. Gong, H. Wang, X. Xu, G. Zhou, Z.S. Wang, In situ growth of Co<sub>0.85</sub>Se and Ni<sub>0.85</sub>Se on conductive substrates as high-performance counter electrodes for dye-sensitized solar cells. *J. Am. Chem. Soc.* **134**(26), 10953–10958 (2012). doi:[10.1021/ja303034w](https://doi.org/10.1021/ja303034w)
46. J.D. Roy-Mayhew, D.J. Bozym, C. Punckt, I.A. Aksay, Functionalized graphene as a catalytic counter electrode in dye-sensitized solar cells. *ACS Nano* **4**(10), 6203–6211 (2010). doi:[10.1021/nn1016428](https://doi.org/10.1021/nn1016428)
47. Y.M. Xiao, J.Y. Lin, S.Y. Tai, S.W. Chou, G. Yue, J.H. Wu, Pulse electropolymerization of high performance PEDOT/MWCNT counter electrodes for Pt-free dye-sensitized solar cells. *J. Mater. Chem.* **22**, 19919–19925 (2012). doi:[10.1039/c2jm34425d](https://doi.org/10.1039/c2jm34425d)
48. L. Han, N. Koide, Y. Chiba, A. Islam, T. Mitate, Modeling of an equivalent circuit for dye-sensitized solar cells: improvement of efficiency of dye-sensitized solar cell by reducing internal resistance. *C. R. Chim.* **9**(5–6), 645–651 (2006). doi:[10.1016/j.crci.2005.02.046](https://doi.org/10.1016/j.crci.2005.02.046)